Two-dimensional electron-momentum densities from angular-correlation measurements of Compton scattering

Thomas Tschentscher and Jochen R. Schneider
Hamburger Synchrotronstrahlungslabor (HASYLAB) at Deutsches Elektronen-Synchrotron (DESY), Notkestrasse 85, 22607 Hamburg, Germany

Friedhelm Bell
Sektion Physik, Universität München, Am Coulombwall 1, 85748 Garching, Germany
(Received 2 April 1993)

The angular correlation between Compton scattered photons and the recoil electrons has been measured in thin self-supporting carbon and aluminum foils using 100-keV synchrotron radiation from a wiggler at the DORIS III storage ring at Deutsches Elektronen-Synchrotron (DESY). The coincidence count rate is proportional to the three-dimensional electron momentum density (3D EMD) of the target, after integration over the energy distribution of the scattered photons and electrons it is proportional to the 2D EMD. The effect of multiple scattering of the recoil electrons within the target on the measured angular correlation is studied both by Monte Carlo calculations and by experiment.

I. INTRODUCTION

Deep inelastic photon scattering of hard x rays has been developed as a tool to study the ground-state electron momentum density (EMD) of solids. In a conventional Compton scattering experiment the energy distribution of the photons scattered at a fixed angle can be related to the so-called Compton profile, which represents a two-dimensional (2D) momentum integration over the EMD perpendicular to the scattering vector. This integration results from the fact that in conventional Compton scattering no information about the momentum of the recoil electron is obtained. Since the main interest of solid-state physicists is in the 3D EMD itself, it has been a long-standing aim to specify the complete scattering kinematics by measuring the energy of the Compton scattered photon in coincidence with the recoiling electron, which makes a direct determination of the ground-state EMD possible. The corresponding technique has been named $(\gamma,e\gamma)$ spectroscopy.[1]

From the beginning it was recognized that strong incoherent elastic scattering of the recoiling electron at the screened nuclei of the target alters the direction of the emerging electron. This effect of multiple scattering introduces uncertainties in the reconstruction of the initial electron momentum. Therefore, very thin target foils have to be used and samples of light materials are preferred, so that the mean free path for electrons with energies in the range of several tens of keV is about a few tens of nm. It is for this reason, together with the small value of the Klein-Nishina cross section, which leads to extremely low count rates, that such coincidence experiments where thought to be impossible. However, the availability of powerful synchrotron-radiation beams with high photon energies from lepton storage rings has changed the situation and recently we have been able to demonstrate the feasibility of such experiments.[1–4]

If the energy of the Compton scattered photon is measured in a coincidence experiment the count rate is proportional to the 3D EMD. To improve the counting statistics it can be advantageous to integrate over the photon and electron energies, so that only the angular correlation of the Compton scattered photon and the corresponding recoil electron are measured. In this case a 2D EMD is measured and the technique may be called "angular correlation of inelastic photon scattering" (ACIPS). The idea of fixing the scattering kinematics by a coincidence condition is already realized in binary $(e,2e)$ spectroscopy and angular-correlation experiments with positron annihilation radiation (ACAR), which are powerful tools for probing ground-state wave functions and/or Fermi surface topology, respectively.

$(e,2e)$ scattering has been widely applied to study electron-momentum distributions in free atoms and molecules; see, e.g., the review paper by McCarthy and Weigold.[5] In contrast, only a few case studies have been performed on solid targets such as carbon[6–11] and aluminum[6,12,13] using this technique. Special interest in $(e,2e)$ scattering arises because it is possible to perform state-dependent spectroscopy by energy discrimination because of the large intrinsic cross section combined with high-electron-beam currents. On the other hand, $(e,2e)$ scattering experiments are even more sensitive to multiple scattering because both collision partners are electrons.

For solids the other alternative to ACIPS is 2D ACAR measurements. These experiments have reached high momentum space resolution, but they measure the EMD weighted by the positron wave function.[14] Especially in a layered structure such as graphite, pronounced differences between the results from ACAR and ACIPS are expected.[15] In graphite the positron stays preferentially in the interlayer region and annihilates more likely with π than with σ electrons,[6–18] making the ACAR

0163-1829/93/48(23)/16965(9)/$06.00

profile narrower than the ACIPS profile. The great affinity of positrons for low-density regions causes a high sensitivity to trapping at defects and complicates the analysis of the experimental data in terms of electron momentum densities. This problem was of special importance in ACAR studies of high-T_c superconductors, suggesting that several features of the measured electron-positron momentum density do not reflect intrinsic properties of the electron momentum density.[19]

In the present paper we report on ACIPS experiments performed on thin foils of carbon and aluminum, both systems having been studied extensively by means of conventional Compton scattering.[20,21] The paper is organized as follows: after a short analysis of the kinematics in ACIPS spectroscopy and a description of the experimental setup, the effect of multiple scattering is discussed by means of Monte Carlo calculations; finally, the experimental results are presented and compared with theory.

II. KINEMATICS

If a high-energy photon is scattered at a free electron initially at rest, the scattered photon energy will be[1]

$$\omega_0'=\omega/[1+\omega(1-\cos\theta)/c^2] . \quad (1)$$

ω is the primary photon energy and θ the scattering angle. We use atomic units, $e=\hbar=m=1$, i.e., the velocity of light is $c=137$. At the same time the recoiling electron will be ejected at an angle ϕ_0 with respect to the primary beam direction where

$$\cot\phi_0=(1+\omega/c^2)\tan(\theta/2) . \quad (2)$$

The influence of an initial electron momentum $\mathbf{p}\neq 0$ is twofold: scattered photons have energies ω' different from ω_0' and recoiling electrons appear at angles ϕ different from ϕ_0. The momentum component p_z parallel to the momentum transfer vector $\mathbf{K}=\mathbf{k}-\mathbf{k}'$ ($\mathbf{k},\mathbf{k}'$ are the momenta of the primary and scattered photons, respectively) introduces a kind of Doppler broadening $\Delta\omega'$ in the energy distribution of the scattered photons:

$$\Delta\omega'=\frac{\omega_0'}{\omega}Kp_z , \quad (3)$$

with $\Delta\omega'=\omega'-\omega_0'$. The components $p_{x,y}$ perpendicular to $\mathbf{K}$ with p_x parallel and p_y perpendicular to the scattering plane ($\mathbf{k},\mathbf{k}'$) are related to the angular deviations $\Delta\phi_{x,y}$ from ϕ_0 by

$$\Delta\phi_{x,y}=p_{x,y}/K . \quad (4)$$

In Eq. (3) binding-energy effects[1] have been neglected. This is a very good approximation for both carbon and aluminum. Thus, by measuring both the Doppler broadening $\Delta\omega'$ and the angular correlation $\Delta\phi_{x,y}$ in a coincident mode, the complete EMD $\rho(p_x,p_y,p_z)$ can be determined.

Since the experiment suffers from low count rates—see Sec. III—we usually decided to integrate over the energy distribution of the photons and electrons and to measure the angular correlation only. It is evident from Eq. (3) that this results in a p_z integration, i.e., the relevant quantity is the angular correlation profile

$$I(p_x,p_y)=\int\rho(p_x,p_y,p_z)dp_z . \quad (5)$$

In this mode ACIPS measurements are very similar to those of ACAR. One may ask whether, in fact, the coincidence count rate is proportional to $I(p_x,p_y)$, i.e., does the cross section for angular correlation factorize in a cross-section part and $I(p_x,p_y)$ even if the validity of the impulse approximation is assumed. It is a question similar to that discussed by Ribberfors[22] in the case of Compton profile measurements. We have investigated the factorization for the experimental situation described below and found that the difference between the factorized and nonfactorized forms of the cross section amounts to at most 5% for transverse momenta up to 5 a.u. This is well within our experimental error bars.

III. EXPERIMENT

The experiment was performed using the radiation from a 56-pole wiggler at the new DORIS III storage ring at Deutsches Elektronen-Synchrotron (DESY), Hamburg. Figure 1 shows the experimental setup. The white wiggler beam was monochromatized by a focusing asymmetrically cut Si crystal[23] in (220) Laue geometry to a monochromaticity of $\Delta\omega=0.5$ keV at $\omega=100$ keV. The monochromated x-ray beam entered an evacuated target chamber with an externally mounted intrinsic Ge diode [energy resolution ~ 0.5 keV full width at half maximum (FWHM) at 100 keV, solid angle ~ 0.4 msr] at $\theta=140°$. A linear array of 7 *PIN* diodes (energy resolution ~ 5 keV FWHM) was placed with its center at $\phi_0=17°$ and could be rotated by 90°, thus allowing p_x and p_y scans. Each *PIN* diode was equipped with its own electronic circuit. According to the dimensions of each *PIN* diode the p_x,p_y resolution was about 0.5 a.u. Since for the conditions mentioned above the modulus of the momentum transfer vector is about 44 a.u., momentum components $p_{x,y}=1$ a.u. correspond to an angular deviation $\Delta\phi_{x,y}=23$ mrad. The scattered photon energy is $\omega_0'=74$ keV and the electron recoil energy 26 keV. With a wiggler gap of 30 mm and an electron energy of 4.5 GeV the critical energy is about 15.8 keV. From the intensity of the Compton scattered photons an incident flux of 1×10^{11} photons/s is derived using the Klein-Nishina

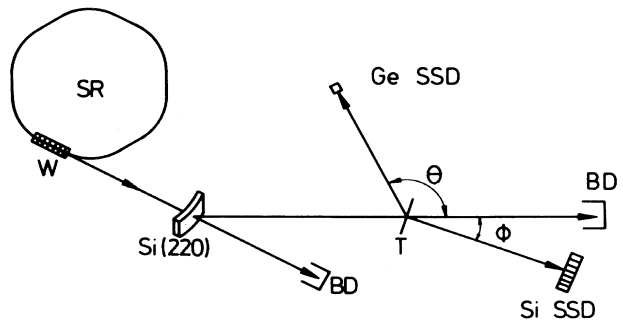

FIG. 1. The experimental setup. SR, storage ring; *W*, wiggler; Si(220), monochromator; BD, beam dumps; *T*, target; Si SSD, electron detector; Ge SSD, photon detector.

cross section. This flux holds for a storage-ring current of 40 mA. With regard to remarks in the introduction about the possibility of ACIPS experiments with conventional radioactive sources we mention that a photon beam of the same flux and an angular divergence of about 10×10 mrad^2 would require a γ activity of 10^{16} Bq.

The storage ring was run in the single-bunch mode with a bunch length of 150 ps and a bunch distance of 960 ns. The time resolution of the coincidence circuit ($\sim$200 ns) is long compared to the former and short compared to the latter. Under these conditions the accidental events are determined by the bunch interval time rather than the time resolution of the electronics.[2] The time spectrum showed no uncorrelated events in neighboring bunches, $\pm$960 ns away from the prompt peak. The maximum coincidence count rate per *PIN* diode was about 100 counts/h.

Both the carbon and the aluminum self-supporting foils have been made by the evaporation-condensation technique. The foil thicknesses were between 5, 40, and 90 μg/cm^2 for carbon, 24 and 500 μg/cm^2 for aluminum. (Assuming for the carbon foils the density of graphite, this corresponds to 22, 180, and 400 nm for carbon, 90 nm and 1.85 μm for aluminum.) The thickness was determined either by light absorption or by weighting and the error is estimated to be about 10%. The carbon foils have also been investigated by Rutherford backscattering (RBS) of 2-MeV α particles. They confirmed the thickness cited above within an error of about 10% and allowed, in addition, an analysis of the thickness fluctuations. Assuming a Gaussian distribution of thicknesses we obtained a standard deviation of 4 μg/cm^2 for the 40-μg/cm^2 foil (i.e., the foil is rather homogeneous) and of 17 μg/cm^2 for the 90-μg/cm^2 foil. In the case of the thinnest foil, the energy resolution of the α-particle detector did not allow such an analysis. These fluctuations, which are seen by an impinging projectile beam, can be induced by surface roughness of a flat foil and/or by waviness of an otherwise homogeneous foil. By comparing the total Rutherford scattering yield with the mean energy loss of the α particles, it was possible to discriminate between both cases and to determine that the foils are flat but rough. The crystallographic structure of the carbon foils has been investigated thoroughly by electron diffraction.[24] From the diffuseness of the diffraction pattern an average size of the crystallites of about 1 nm was derived. For carbon foils prepared by thermal evaporation the small dimensions of the crystallites lead to the assumption that the foils are amorphous,[25] although electron diffraction shows an anisotropic structure that contradicts an amorphous state. It is generally assumed that in evaporated carbon a substantial degree of medium-range order on the 1-nm scale exists: the sp^2 sites of carbon atoms tend to occur in warped graphite layer clusters.[26] Heat treatment up to 2200 K made the diffraction rings of our foils sharper and showed clearly a graphitic pattern with the basal planes oriented randomly parallel to the surface of the foils.

It is well known that aluminum metal readily oxidizes at its surface, forming alumina with a thickness of about 1.5–3 nm.[13] This saturated oxide layer is small compared to the thickness of the thinnest aluminum foil of about 90 nm used in the present experiment.

Elastic recoil detection analysis with 120-MeV ^{127}I ions from the Munich heavy-ion accelerator revealed that the major contaminant of the carbon foils is water molecules on the surfaces that cannot be desorbed even in vacuum.[27] This water film amounts to about 0.05 molecules per carbon atom for the 5-μg/cm^2 carbon foil and is assumed to form a layer of constant thickness for all carbon and aluminum foils.

IV. MONTE CARLO CALCULATION

As already discussed in the Introduction, the emerging recoil electrons might suffer from elastic scattering even in very thin foils. It turns out that for 26-keV electrons the mean free path λ_e for elastic scattering is about 8.2 μg/cm^2 in carbon and 7.5 μg/cm^2 in aluminum. Thus, for most of our foils the vast majority of the electrons will undergo plural or even multiple scattering. We have therefore written a Monte Carlo code to simulate the emission process. In order to obtain high accuracy based on a large number of trajectories (1×10^7), we decided not to simulate the whole experiment by a Monte Carlo calculation but only the emission of those electrons that started randomly within the foil with a direction parallel to the momentum transfer vector **K**. Since in the experiment the foils are tilted with their surface normal parallel to **K**, the simulation process exhibits cylindrical symmetry that facilitates the calculation. The distribution function $g(\mathbf{p}_\perp)$ is given in terms of transverse momenta $p_\perp=(p_x^2+p_y^2)^{1/2}$, which are the momenta of the electrons when leaving the foil. Distributions $\langle A(\mathbf{p}_\perp,p_z)\rangle$ smeared by multiple scattering can be obtained from the undisturbed distribution $A(\mathbf{p}_\perp,p_z)$ by a simple two-dimensional convolution

$$\langle A(\mathbf{p}_\perp,p_z)\rangle = P_0 A(\mathbf{p}_\perp,p_z) + (1-P_0-P_r)\int A(\mathbf{p}_\perp-\mathbf{p}'_\perp,p_z) \times g(\mathbf{p}'_\perp)d^2p'_\perp , \quad (6)$$

where the scattering function $g(\mathbf{p}_\perp)$ is normalized to unity

$$\int g(\mathbf{p}_\perp)d^2\mathbf{p}_\perp=1 , \quad (7)$$

P_0 is the fraction of unscattered electrons and P_r that of backscattered electrons. The distribution A can be either the EMD $\rho(\mathbf{p}_\perp,p_z)$ or the angular-correlation profile $I(\mathbf{p}_\perp)$ of Eq. (5). Details of the Monte Carlo procedure can be found in Ref. 2. For the elastic scattering cross section we used the Mott-Born expression

$$\frac{d\sigma^{\mathrm{MB}}}{d(q^2)}=\pi\left[\frac{2Z}{vq^2}\right]^2[1-(q/2\gamma c)^2]\left[1-\frac{F(q)}{Z}\right]^2 , \quad (8)$$

where Z is the nuclear charge of the target, v the electron velocity, and $q=2p\sin(\alpha/2)$ the momentum transfer. p is the momentum of the recoiling electron and α the electron scattering angle. $\gamma=[1-(v/c)^2]^{-1/2}$. Salvat *et al.*[28] have evaluated the atomic form factor $F(q)$ for a

Dirac-Hartree-Fock-Slater atom and write it in the form

$$\frac{F(q)}{Z}=\sum_{i=1}^{3} A_i\alpha_i^2/(\alpha_i^2+q^2) . \tag{9}$$

The parameters A_i,α_i have been tabulated for all atoms with $Z=1-92$.[28] The mean free path λ_e is obtained from $\lambda_e=(N\sigma)^{-1}$ with the number density of the target atoms N, and the total cross section

$$\sigma=\int_0^{(2p)^2}\frac{d\sigma^{\mathrm{MB}}}{d(q^2)}d(q^2) . \tag{10}$$

Figure 2 shows the normalized scattering function $g(p_\perp)$ for five different carbon foil thicknesses. The curves have not been smoothed, and the nearly invisible wiggles on the curves reflect the high statistical accuracy of the Monte Carlo procedure. For the thickest foil (1 mg/cm^2) a cutoff at $p_\perp=p=44$ a.u. is observed. Since no electrons with total scattering angles larger than 90° can leave the foil in the forward direction, those are defined to be backscattered. For 1 mg/cm^2 this fraction is about $P_r=0.12$. Figure 3 demonstrates how the multiple scattering of the recoiling electrons disturbs, for instance, the angular-correlation profile $I(p_\perp)$. Very recently, Yongming, Johansson, and Nieminen[29] have calculated 3D and 2D EMD's of graphite using an empirical pseudopotential method. Assuming the basal plane of graphite to be parallel to the foil surface with otherwise randomly distributed crystallites, we have azimuthally averaged $I(p_x,p_y)$ and folded with the multiple-scattering function $g(p_\perp)$. In Fig. 3 $\langle I(p_\perp)\rangle$ is plotted for three different carbon-foil thicknesses (solid lines). The contribution of scattered electrons, i.e., the second term of Eq. (6), is indicated by broken lines. The sharp drop of the profile at about $p_\perp=0.8$ a.u. occurs at the M point of the Brillouin-zone face in the $\langle 1100\rangle$ direction and is still visible after the azimuthal averaging. This drop is characteristic for layered structures of semiconductors and insulators with large layer separations. It is interesting to note that this distinct feature of $I(p_\perp)$ is even visible at a thickness d where $d/\lambda_e=114$ ($d=1$ mg/cm^2). This is because of the fact that for small transverse momentum ($p_\perp<0.8$ a.u.) the contribution of the unscattered electrons to $\langle I(p_\perp)\rangle$ still amounts to about 40%, although the total fraction P_0 is 0.9% only, where, according to Poisson statistics,

$$P_0=\frac{\lambda_e}{d}[1-\exp(-d/\lambda_e)] . \tag{11}$$

In other words, the scattered electrons are smeared over a rather large $p_\perp$ range, leaving a small contribution at low $p_\perp$ values only. This situation, which is reminiscent of a last-layer effect, is more quantitatively demonstrated in Fig. 4. Here, we have plotted $dI_1(0)$ (triangles) and $dI_2(0)$ (circles) as a function of d/λ_e. $I_{1,2}(0)$ are the first and second part of the sum in Eq. (6) for $p_\perp=0$, i.e., the yield of unscattered and scattered electrons at zero transverse momentum. The squares represent the total yield $d\langle I(0)\rangle=d[I_1(0)+I_2(0)]$. The dashed curve is the theoretical expression for $dP_0I(0)$. The points result from Monte Carlo calculation and the straight lines are guides to the eye. It is evident that the contribution of

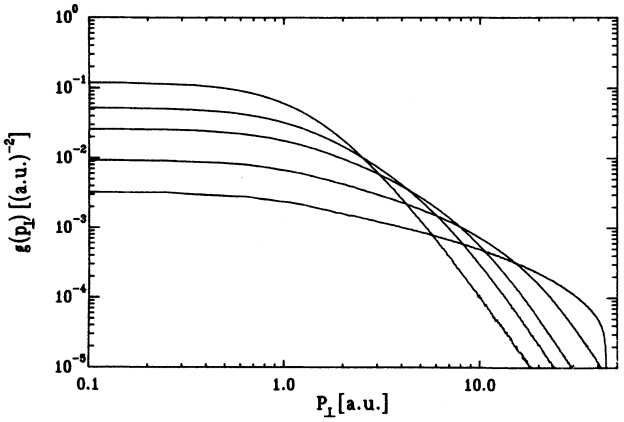

FIG. 2. The normalized multiple-scattering function $g(p_\perp)$ for a 5-, 40-, 90-, 280-, and 1000-μg/cm^2-thick carbon foil (from top to bottom).

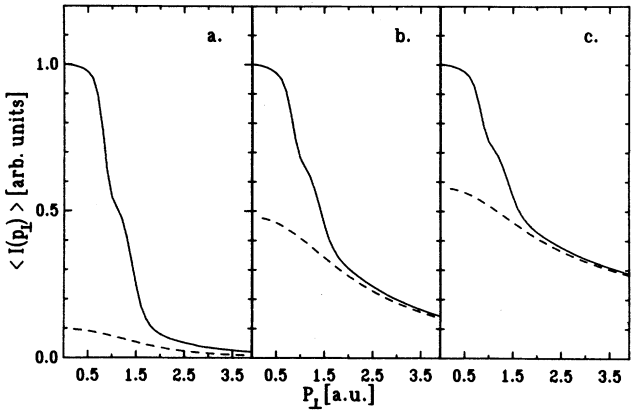

FIG. 3. The theoretical angular-correlation profile $\langle I(p_\perp)\rangle$ of a 5- (a), 90- (b), and 1000- (c) μg/cm^2-thick carbon foil (solid lines). The broken lines show the contribution of scattered electrons. The peak value is normalized to one.

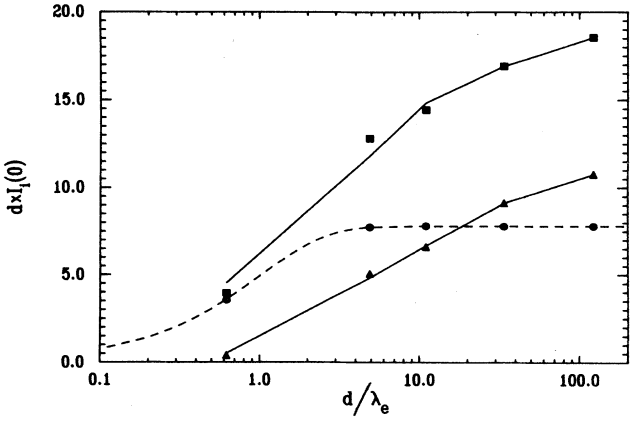

FIG. 4. The coincident electron yield $dI_i(0)$ for the unscattered (circles) and scattered (triangles) electrons at $p_\perp=0$ as a function of d/λ_e. The squares represent the sum, i.e., the total yield. The dashed curve is the theoretical expectation from Poisson statistics.

scattered electrons increases slowly and equals the unscattered part at $d/\lambda_e \cong 20$. It is tempting to conclude that if one is interested only in distinct features such as the Fermi surface with sharp breaks in the momentum density, even foil thicknesses up to a hundred times the mean free path of elastic scattering are useful. This facilitates such experiments tremendously.

The form factor of Eq. (9) with coefficients from Ref. 28 corresponds to an isolated atom. In contrast, one can argue that in solids the nuclear charge Z is completely screened by the electrons within the Wigner-Seitz cell.[30,31] Salvat and Paralleda[31] have evaluated form factors for solids under appropriate boundary conditions. We have calculated $\langle I(p_\perp)\rangle$ for a 24-μg/cm^2 aluminum foil with both an atomic and a solid-state form factor. Figure 5 shows the result. The difference in the two profiles is mainly due to a slight increase in the fraction of unscattered electrons in the case of the solid-state target. Since the interaction potential becomes constant for distances larger than the Wigner-Seitz radius, the total cross section is reduced. As shown in the next section, the accuracy of our present data is too low to allow discrimination between these effects, but we admit that with increasing accuracy a problem may emerge. Since for the evaluation of solid-state cross sections single-collision conditions cannot be realized, a sound experimental test of this cross section does not exist so far.

In our Monte Carlo calculation it is assumed that the angular spreading of the electrons is dominated by incoherent elastic scattering and that the influence of inelastic scattering, both on angular dispersion and slowing down of the electrons, can be neglected. The first assumption is usually justified by the Z dependence of the cross sections;[2,31,32] the second is peculiar to our experimental situation: due to the compilation of Pages *et al.*[33] the average energy-loss rate of 26 keV electrons amounts to 9.9 eV cm^2/μg in carbon and 8.3 eV cm^2/μg in aluminum. Thus, even for the thick aluminum foil (500 μg/cm^2) the mean energy loss is less than the energy resolution of our electron detector. A rough estimate may support the first assumption: the mean free path for inelastic scattering in aluminum[34] at 26 keV is about 8.9 μg/cm^2 and thus very similar to that for elastic scattering (7.5 μg/cm^2). For the energy-loss data cited this corresponds to an average energy loss of $\Delta E = 73$ eV, which, in turn, means a r.m.s. deflection angle for inelastic scattering of $\theta_{\text{inel}} \cong \Delta E/(pv) = 1.4$ mrad.[35] In contrast, we calculate from the cross section of Eq. (8) a r.m.s. angle for elastic scattering of about 80 mrad, which is more than a factor 50 larger than θ_{inel}. The situation for carbon is similar.[36]

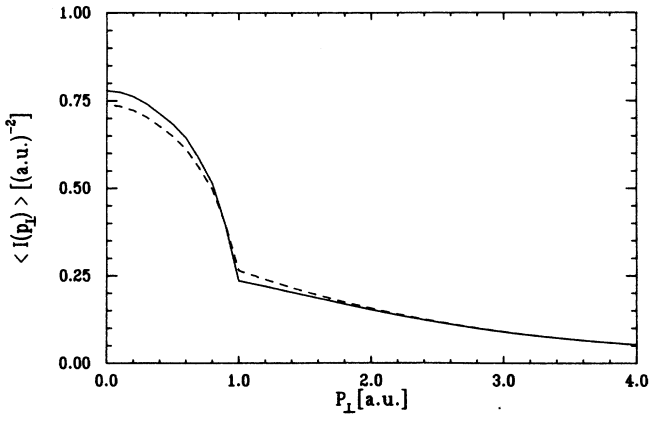

FIG. 5. A comparison of the angular correlation profiles $\langle I(p_\perp)\rangle$ for a 24-μg/cm^2 aluminum foil obtained from atomic (broken curve) or solid-state cross sections (solid curve).

It might be appropriate at this stage of the discussion to say a few words about coherent scattering of both the incoming photon and the recoiling electron. Since for 100-keV photons the extinction length is orders of magnitude larger than our foil thicknesses,[37] the coherent scattered intensity is negligibly small compared to the primary intensity. The situation is completely different for the electrons where both length scales become comparable.[32] Coherent scattering of the recoil electrons would force them into certain directions. In a single crystal one would expect defect or excess Kikuchi bands superimposed on a background of incoherently scattered electrons. At high electron energies the emission pattern can be interpreted in terms of electron channeling or blocking based on a many-beam analysis of the dynamical theory of diffraction.[32,38] To give an example, the width of a Kikuchi band, which is two times the Bragg angle θ_B, yields for the (220) plane in aluminum $\Delta p_\perp = 2\theta_B K = g_{220} = 2.33$ a.u. g_{220} is the modulus of the corresponding reciprocal lattice vector. However, since Kikuchi patterns are fixed to the crystal lattice, they would be smeared out in a polycrystalline target. Based on this heuristic argument coherent scattering has been disregarded in this work. The effect of diffraction on the $(e,2e)$ reaction in crystals has also been discussed by Allen *et al.*[39] Finally, we mention that the situation partly resembles x-ray photoelectron diffraction, which is by now a well-established technique for the elucidation of the surface structure of epitaxially grown thin films.[40] In this case also, the emission pattern has been related to Kikuchi band formation,[41] especially if the core-level photoelectrons originate from atoms rather deep in the lattice.[42]

V. RESULTS AND DISCUSSION

Figure 6 shows the experimental angular correlation profile for a scan parallel (triangles) and perpendicular (circles) to the $(\mathbf{k},\mathbf{k}')$ scattering plane. The target was a 5-μg/cm^2 foil. The experimental data points are compared with a theoretical $\langle I(p_\perp)\rangle$ curve (solid line) where the contribution of the $(1s)^2$ core has been added to the $I(p_\perp)$ data for the valence electrons.[29] The $(1s)^2$ core was calculated from Roothaan-Hartree-Fock wave functions of Clementi and Roetti.[43] After correction for multiple scattering described in Sec. IV, the calculated $\langle I(p_\perp)\rangle$ has been averaged over the finite acceptance angle of the electron detector. This corresponds to a smearing of the profile over a range of ± 0.25 a.u. It turns out that this averaging procedure destroys the steplike character of the angular correlation profile of Fig. 3. As indicated in Sec. III, there might exist some doubts about the crystal-

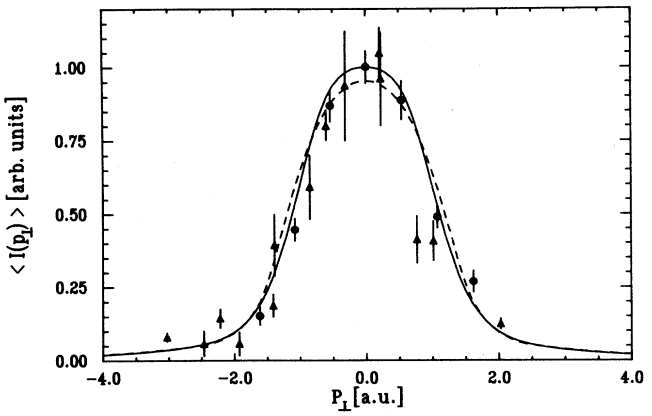

FIG. 6. The angular-correlation profile of a 5-μg/cm^2 carbon foil for a scan within the scattering plane (triangles) and perpendicular to it (circles). The data points are compared with theoretical profiles for graphite (solid line) from Ref. 29 and diamond (broken line) from Ref. 44.

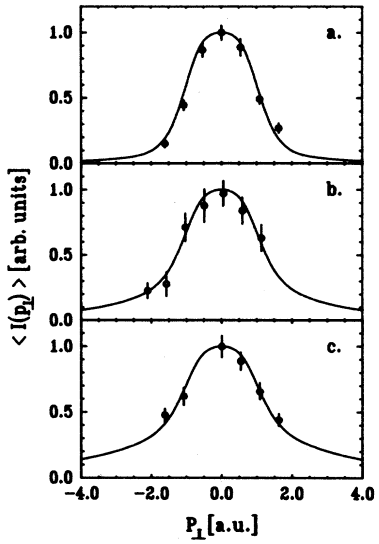

FIG. 7. Angular correlation profiles for a 5- (a), 40- (b), and 90-μg/cm^2 (c) -thick carbon foil. The theoretical curves have been fitted to the data points with a constant factor for each data set.

linity of evaporated carbon foils. Nevertheless, the band structure of amorphous carbon still resembles gross features of the crystalline solid as emphasized by Hayes *et al.*[13] Employing the $(e,2e)$ technique, Hayes, Williams, and Flexman[6] compared a graphite foil with a more amorphous carbon foil and found no major difference. Although recent $(e,2e)$ experiments[7] on evaporated carbon foils revealed that the electronic structure consists predominantly (85–100 %) of graphitic sp^2 bonding, we also compare the data with a $\langle I(p_\perp)\rangle$ curve (broken curve) obtained from a spherically averaged EMD of diamond.[44] As expected, no difference in the experimental data for the p_x and p_y scan can be seen within statistical accuracy. Nevertheless, scans of this kind are a very useful check of the adjustment of the electron detector: the linear detector array has to be adjusted within ± 10 mrad in both directions to hit the center of the $\langle I(p_\perp)\rangle$ distribution. Figure 7 shows the influence of multiple scattering: experimental data points for 5-, 40-, and 90-μg/cm^2 carbon foils are compared with theoretical $\langle I(p_\perp)\rangle$ curves. As in Fig. 6, the experimental points are on a relative scale, i.e., theory has been fitted to the data by a common factor for each curve. The broadening of the distribution due to multiple scattering of the emerging electron is clearly observed. Nevertheless, in the future more data points at higher p_x values need to be measured.

A more stringent test of the multiple-scattering theory is a comparison of the absolute yield for different foil thicknesses. Figure 8 shows the coincidence count rate for a 40- and a 90-μg/cm^2 carbon foil normalized to the total photon singles yield measured simultaneously. Thus, if there would be no multiple electron scattering at all, both experimental curves should be identical. In fact, the normalized count rate of the thicker foil decreases roughly by a factor of 2. Since the foil thickness has increased by about the same factor, the coincidence count rate stays approximately constant when going from a 40- to a 90-μg/cm^2 foil. Again, the solid curves represent the results from Monte Carlo calculations that have been fitted to the data with one scale factor for both curves. The 5-μg/cm^2 foil data do not agree that well with the calculation. Without multiple scattering the total coincidence count rate should increase by a factor of 18 by going from 5 to 90 μg/cm^2. From theory the inclusion of multiple scattering is expected to reduce the gain in total coincidence count rate to a factor of 4.0, whereas the experiment yields a factor of 6.6 ± 2.0. Compared to Figs. 6 and 7, the uncertainties of the photon yield and the foil thickness increase the experimental error.

In a long-time run (16 h) we also measured the 3D EMD by recording Doppler-broadened x-ray events in coincidence with electron events in the central pixel of the *PIN* diode array. Thus, the count rate is proportional

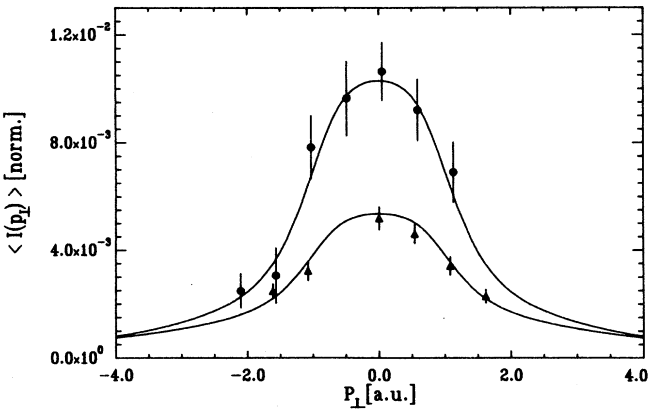

FIG. 8. Angular-correlation profiles normalized to the photon singles yield for a 40-μg/cm^2 (circles) and a 90-μg/cm^2 carbon foil (triangles). The theoretical curves are fitted to the data by a common factor.

to $\rho(0,0,p_z)$, where the zeros are understood within the experimental resolution of $\Delta p_x = \Delta p_y = \pm 0.25$ a.u. In Fig. 9 the result for a 5-μg/cm^2 carbon foil is compared with two theoretical $\langle \rho(0,0,p_z) \rangle$ curves, one for the azimuthally (solid), the other for the spherically (dotted) averaged EMD of Ref. 29. In addition, these curves have been folded with an experimental p_z resolution of 0.7 a.u. Whereas, in general, the agreement is quite good, there might be a small discrepancy for $p_z \cong 0$. The theoretical 3D EMD data of Yongming, Johansson, and Nieminen[29] show a strong bimodal structure in the direction of the c axis with a saddle point nat $p=0$. This anisotropy results primarily from the π band (and probably contributions from the p character of the σ_2 and σ_3 bands near the Brillouin-zone center[45]) and is clearly observed in 1D or 2D ACAR measurements.[16–18] Interestingly, the lobes of this structure survive the spherical averaging. Although the "discrepancy" of Fig. 9 relies on one data point only with a rather large error, theory also seems to be flexible. Apparently, there exists a range of acceptable parameters of the pseudopotential for which the bimodal shape even disappears.[29] As mentioned in the Introduction, the structure found in ACAR measurements can be strongly enhanced due to preferential positron annihilation at π electrons. An indication for an exaggerated bimodal structure seems to be that even the directional Compton profile $J(p_z)$ from Ref. 29 with $p_z \| \langle 0001 \rangle$ shows a dip at $p_z = 0$, in contrast to the result from Chou, Cohen, and Louie,[46] who also used a pseudopotential local-density-functional calculation. In addition, the theoretical difference[29] $J_{\|c} - J_{\perp c}$ with p_z parallel and perpendicular to the c axis is by far more pronounced at $p_z \cong 0$ than observed experimentally by Vasudevan *et al.*[20] and Tyk *et al.*[20]

It is unlikely that an amorphous state of the foil could alter the EMD, especially at low momenta. In theory,[47] close to the center of the Brillouin zone, the long-wavelength states depend on an averaged crystal structure that will be similar in both the crystalline and amorphous states of carbon. A comparison of the density of states (DOS) at the bottom of the σ_1 band for a continuous random network of amorphous graphite[48] with that for crystalline graphite[49] shows virtually no difference. In both cases one observes the same step-function-like onset of the DOS characteristic of a two-dimensional behavior, in clear contradiction to a square-root dependence on energy[49] as observed for nearly free electrons in three dimensions. Molecular-dynamics (MD) calculations by Galli *et al.*[50] revealed that amorphous carbon is arranged in so-called "thick planes" reminiscent of the stacking sequence in crystalline graphite. Although most of the bonds formed by sp^2 atoms tend to lie nearly on the same plane as in graphite, substantial buckling occurs locally, which yields thick planes with a finite thickness of about 1.0–1.2 a.u. The steplike character of the DOS is also revealed by MD calculations of Blaudeck *et al.*[51] A detailed discussion of the electronic structure of amorphous carbon can be found in the review article of Robertson.[26]

In Fig. 10 we show angular correlation profiles for 24- and 500-μg/cm^2-thick aluminum foils. For the theoretical profile $I(p_\perp)$ we use for the valence electrons a Fermi sphere with radius $p_F = 0.93$ a.u. (Shiotani *et al.*[21]) and for the $(1s)^2(2s)^2(2p)^6$ core the Roothaan wave functions of Clementi and Roetti.[43] The free-electron model is a very good approximation for aluminum as shown by augmented-plane-wave calculations of Kubo, Wakoh, and Yamashita[52] and is further supported by experiment because no anisotropies of directional Compton profiles could be detected within the experimental accuracy.[21,53] Very small anisotropies of the Fermi surface ($p_F[100] = (0.922 \pm 0.004)$ a.u., $p_F[110] = (0.914 \pm 0.011)$ a.u., and $p_F[111] = (0.930 \pm 0.005)$a.u.) have been observed by 2D ACAR measurements[54] and should be compared with the free-electron value of $p_F = 0.929$ a.u. As discussed in Sec. IV, even for the 500-μg/cm^2 foil ($d/\lambda_e = 66$) the discontinuity of the solid curve at the Fermi momentum is clearly visible, although $\langle I(p_\perp) \rangle$ has

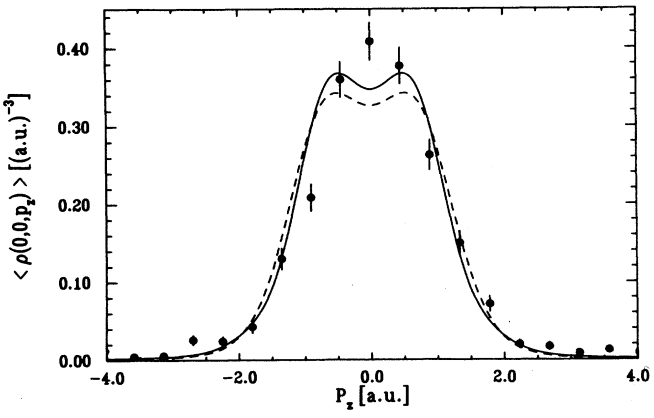

FIG. 9. The momentum density $\langle \rho(0,0,p_z) \rangle$ for a 5-μg/cm^2 carbon foil. For comparison, the spherically (broken curve) and azimuthally (solid curve) averaged EMD from Ref. 29. Theory has been convoluted with a Gaussian with 0.7 a.u. FWHM.

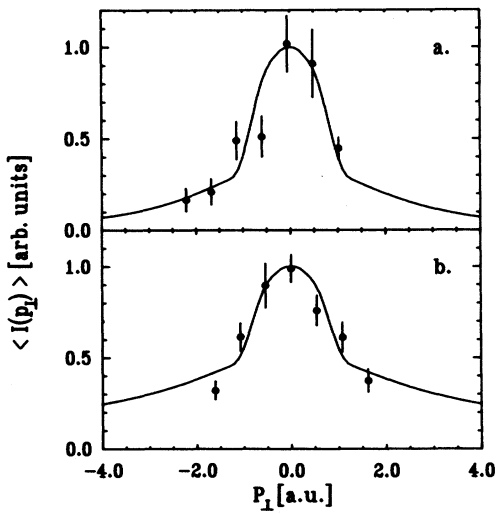

FIG. 10. Angular correlation profiles for a 24-μg/cm^2 (a) and 500-μg/cm^2 (b) -thick aluminum foil. The solid curves are from theory.

been averaged over 0.5 a.u.

The results for carbon and aluminum illustrate both the advantages and disadvantages of ACIPS measurements. In fact, it has been shown that such measurements are possible using synchrotron radiation from storage rings of high electron energy. At the moment, counting statistics are rather poor, so that the experiment can hardly compete with other methods which gain information about the electronic ground state of condensed matter and which have been mentioned in the Introduction. But there is hope that the error bars of Figs. 6–8, which are of a statistical nature only, can be reduced in the near future by increasing the primary photon flux by large amounts. This might be possible using insertion devices at synchrotron-radiation sources such as the European Synchrotron Radiation Facility (ESRF) in Grenoble or the PETRA storage ring in Hamburg operated at 12 GeV electron energy. A calculation[55] of the brightness for an undulator installed at PETRA shows that at a photon energy of 150 keV the fifth harmonic would increase the brightness by more than four orders of magnitude compared to a wiggler at DORIS III. Because the solid angle the PETRA undulator would provide is smaller than that used in our experiment, the effective gain factor is between 10^3 and 10^4. In this context one should mention the disadvantage of pulsed radiation sources for coincidence experiments due to the small duty cycle defined as the ratio of bunch length to bunch interval. However, both machines mentioned above can be operated in a multibunch mode, so that the gain in average intensity is not outweighed by accidental coincidences. As discussed above, the $p_\perp$ resolution of the angular correlation profiles depends on the solid angles of both the electron and x-ray detector and can be improved easily.

A major drawback of the method is the influence of electron multiple scattering, which restricts the measurements to thin self-supporting foils. Since the surface area of the foils should be of the order of 10 mm^2—due to the photon beam dimension—the situation $d/\lambda_e < 1$ can only be fulfilled for carbon. But if one is mainly interested in distinct features such as the Fermi surface (i.e., fermiology)—which resembles for quite different reasons the situation of ACAR measurements—even foils with $d/\lambda_e = 100$ might be useful. A possible solution to the multiple-scattering problem is to go to higher photon energies, i.e., larger electron recoil energies. This means an increase of the mean free path for elastic scattering. Going from 100 to 300 keV photon energy changes the electron energy from 26 to 152 keV, i.e., roughly increases the mean free path by a factor of 6. At the same time, the Klein-Nishina cross section is reduced by a factor of only 2. This is in contrast to the situation of $(e,2e)$ experiments where a similar solution of the multiple scattering problem has been proposed but is accompanied by a drastic reduction of the Mott cross section.[6]

ACKNOWLEDGMENTS

The authors thank A. J. Rollason and M. B. J. Woolf, University of Keele, U. K., for their help in data taking. They are very much indebted to Lou Yongming, University of Missouri–Kansas City, for making available his theoretical EMD of graphite. We also thank G. Dollinger and H. J. Maier from the Munich Target Lab Groups for the preparation of the foils and H. D. Carstanjen, Max-Planck-Institut für Metallforschung, Stuttgart, for the RBS measurements. Finally, thanks are due to P. Suortti, ESRF, Grenoble, for providing the monochromator. This work was supported by the Bundesministerium für Forschung und Technologie, Contract No. 05 5WMAAI.

[1]F. Bell, A. J. Rollason, J. R. Schneider, and W. Drube, Phys. Rev. B **41**, 4887 (1990).

[2]F. Bell, Th. Tschentscher, J. R. Schneider, and A. J. Rollason, J. Phys. Condens. Matter **3**, 5587 (1991).

[3]J. R. Schneider, F. Bell, Th. Tschentscher, and A. J. Rollason, Rev. Sci. Instrum. **63**, 1119 (1992).

[4]Th. Tschentscher, J. R. Schneider, F. Bell, A. J. Rollason, and M. B. J. Woolf, Nucl. Instrum. Methods B **79**, 237 (1993).

[5]I. E. McCarthy and E. Weigold, Rep. Prog. Phys. **54**, 789 (1991).

[6]P. Hayes, F. J. Williams, and J. Flexman, Phys. Rev. B **43**, 1928 (1991).

[7]Chao Gao, Yun Yu Wang, A. L. Ritter, and J. R. Dennison, Phys. Rev. Lett. **62**, 945 (1989).

[8]A. L. Ritter, J. R. Dennison, and R. Jones, Phys. Rev. Lett. **53**, 2054 (1984).

[9]Chao Gao, A. L. Ritter, J. R. Dennison, and N. A. W. Holzwarth, Phys. Rev. B **37**, 3914 (1988).

[10]R. Camilloni, A. Giardini Guidoni, R. Tiribelli, and G. Stefani, Phys. Rev. Lett. **29**, 618 (1972).

[11]J. Lower, S. M. Bharathi, Yu Chen, K. J. Nygaard, and E. Weigold (unpublished).

[12]N. M. Persiantseva, N. A. Krasil'nikova, and V. G. Neudachin, Zh. Eksp. Teor. Fiz. **76**, 1047 (1979) [Sov. Phys. JETP **49**, 530 (1979)].

[13]P. Hayes, M. A. Bennett, J. Flexman, and J. F. Williams, Phys. Rev. B **38**, 13 371 (1988).

[14]S. Berko, in *Positron Solid-State Physics,* Proceedings of the International School of Physics "Enrico Fermi," Course LXXXIII, Varenna, 1981, edited by W. Brandt and A. Dupasquier (North-Holland, New York, 1983), p. 64.

[15]Lou Yongming, B. Johansson, and R. M. Nieminen, J. Phys. Condens. Matter **3**, 2057 (1991).

[16]I. Kanazawa, S. Tanigawa, R. Suzuki, M. Sano, and H. Inokuchi, Phys. Rev. B **42**, 11 583 (1990).

[17]R. R. Lee, E. C. von Stetten, M. Hasegawa, and S. Berko, Phys. Rev. Lett. **58**, 2863 (1987).

[18]S. Berko, R. E. Kelly, and J. S. Plaskett, Phys. Rev. **106**, 824 (1957).

[19]L. C. Smedskjaer and A. Bansil, J. Phys. Chem. Solids **53**, 1657 (1992).

[20]W. A. Reed and P. Eisenberger, Phys. Rev. B **6**, 4596 (1972); R. S. Holt, Solid State Commun. **59**, 321 (1986); S. Vasudevan, T. Rayment, B. G. Williams, and R. Holt, Proc. R. Soc. London Ser. A **391**, 109 (1984); R. J. Weiss and W. C. Philips, Phys. Rev. **176**, 176 (1968); M. Cooper and J. A. Leake, Phi-

los. Mag. **15**, 1201 (1967); R. Tyk, J. Felsteiner, I. Gertner, and R. Moreh, Phys. Rev. B **32**, 2625 (1985); W. A. Reed, P. Eisenberger, K. C. Pandey, and L. C. Snyder, *ibid.* **10**, 1507 (1974); T. L. P. Paakkari, Phys. Fenn. **9**, 185 (1974).

[21]M. Cooper, P. Pattison, and J. R. Schneider, Philos. Mag. **34**, 243 (1976); W. C. Philips and R. J. Weiss, Phys. Rev. **171**, 790 (1968); P. Pattison and B. Williams, Solid State Commun. **20**, 585 (1976); N. Shiotani, N. Sakai, M. Ito, O. Mao, E. Itoh, H. Kawata, Y. Amemiya, and M. Ando, J. Phys. Condens. Matter **1**, 27 (1989); M. Cooper, P. Pattison, B. Williams, and K. C. Pandey, Philos. Mag. **29**, 1237 (1974); P. Pattison, S. Manninen, J. Felsteiner, and M. Cooper, *ibid.* **30**, 973 (1974); S. Manninen, T. Paakkari, and K. Kajante, *ibid.* **29**, 167 (1974); J. L. DuBard, *ibid.* **37**, 273 (1978); R. S. Holt, J. L. DuBard, M. J. Cooper, T. Paakkari, and S. Manninen, Philos. Mag. B **39**, 541 (1979).

[22]R. Ribberfors, Phys. Rev. B **12**, 2067 (1975); **12**, 3136 (1975).

[23]P. Suortti, D. Chapman, J. R. Schneider, and Th. Tschentscher, J. Appl. Crystallogr. **25**, 432 (1992).

[24]G. Dollinger, P. Maier-Komor, and A. Mitwalsky, Nucl. Instrum. Methods A **303**, 79 (1991).

[25]J. Kakinoki, K. Katada, T. Hanawa, and T. Ino, Acta Crystallogr. **13**, 171 (1960).

[26]J. Robertson, Adv. Phys. **35**, 317 (1986).

[27]G. Dollinger and W. Assmann (unpublished).

[28]F. Salvat, J. D. Martinez, R. Mayol, and J. Parellada, Phys. Rev. A **36**, 467 (1987).

[29]Lou Yongming, B. Johansson, and R. M. Nieminen, J. Phys. Condens. Matter **3**, 1699 (1991).

[30]W. Raith, Acta Crystallogr. Sec. A **24**, 85 (1968).

[31]F. Salvat and J. Parellada, J. Phys. D **17**, 1545 (1984).

[32]L. Reimer, in *Transmission Electron Microscopy,* Springer Series in Optical Sciences Vol. 36 (Springer, Berlin, 1984).

[33]L. Pages, E. Bertel, H. Joffre, and L. Sklavenitis, At. Data **4**, 1 (1972).

[34]C. J. Tung, J. C. Ashley, and R. H. Ritchie, Surf. Sci. **81**, 427 (1979).

[35]R. H. Ritchie and A. Howie, Philos. Mag. **36**, 463 (1977).

[36]R. F. Egerton, Philos. Mag. **31**, 199 (1975).

[37]W. H. Zachariasen, *Theory of X-ray Diffraction in Crystals* (Wiley, New York, 1945); Max v. Laue, *Röntgenstrahl-Interferenzen* (Akademische Verlagsgesellschaft, Frankfurt am Main, 1960).

[38]S. K. Andersen, F. Bell, F. Frandsen, and E. Uggerhoj, Phys. Rev. B **8**, 4913 (1973); J. U. Andersen, S. K. Andersen, and W. M. Augustyniak, K. Dan. Vidensk. Selsk. Mat. Fys. Medd. **39** (1977); H. Hofsäss and G. Lindner, Phys. Rep. **201**, 121 (1991).

[39]L. J. Allen, I. E. McCarthy, V. W. Maslen, and C. J. Rossouw, Austr. J. Phys. **43**, 453 (1990); L. J. Allen and C. J. Rossouw, Phys. Rev. B **47**, 2446 (1993).

[40]S. A. Chambers, Adv. Phys. **40**, 357 (1991).

[41]R. Trehan, J. Osterwalder, and C. S. Fadley, J. Electron Spectrosc. Relat. Phenom. **42**, 187 (1987).

[42]W. F. Egelhoff, CRC Crit. Rev. Solid State Mater. Sci. **16**, 213 (1990).

[43]E. Clementi and C. Roetti, At. Data Nucl. Data Tables **14**, 177 (1974).

[44]A. Seth and D. E. Ellis, J. Phys. C **10**, 181 (1977).

[45]N. A. W. Holzwarth, S. G. Louie, and S. Rabii, Phys. Rev. B **26**, 5382 (1982).

[46]M. Y. Chou, M. L. Cohen, and S. G. Louie, Phys. Rev. B **33**, 6619 (1986).

[47]J. M. Ziman, J. Phys. C **4**, 3129 (1971).

[48]A. Gibson and R. Haydock, Phys. Rev. Lett. **69**, 3793 (1992).

[49]J.-C. Charlier, X. Gonze, and J. P. Michenaud, Phys. Rev. B **43**, 4579 (1991); J.-C. Charlier, J.-P. Michenaud, and Ph. Lambin, *ibid.* **46**, 4540 (1992).

[50]G. Galli, R. M. Martin, R. Car, and P. Parrinello, Phys. Rev. B **42**, 7470 (1990).

[51]P. Blaudeck, Th. Frauenheim, D. Porezag, G. Seigert, and E. Fromm, J. Phys. Condens. Matter **4**, 6389 (1992).

[52]Y. Kubo, S. Wakoh, and J. Yamashita, J. Phys. Soc. Jpn. **41**, 830 (1976).

[53]M. Causa, R. Dovesi, C. Pisani, and C. Roetti, Philos. Mag. B **44**, 419 (1981).

[54]J. Mader, S. Berko, H. Krakauer, and A. Bansil, Phys. Rev. Lett. **37**, 1232 (1976).

[55]W. Brefeld and P. Gürtler (unpublished).